

Topological extension including quantum jump

Xiangyu Niu¹ and Junjie Wang¹

¹*Center for Quantum Sciences, School of Physics, Northeast Normal University, Changchun 130024, China.**

(Dated: December 22, 2022)

We study the topological properties of the Su-Schrieffer-Heeger (SSH) model with collective loss and gain. When the system is in the absence of quantum jump events, the dynamic is equivalent to a fully studied non-reciprocal non-Hermitian (NH) SSH model. We unveil the classification of Lindbladians by means of the third quantization and hence define the corresponding winding number. Intriguingly, the two descriptions share the same transition points, and faithfully predict the topology. In addition, when the quantum jumping terms are presented, the phase transition points may shift, which cannot be predicted by the effective NH theory. Our work bridges the NH and open quantum system descriptions in studying the topological properties, and reveals the unique role of quantum jumps.

I. INTRODUCTION

Topological band theory has always played a fundamental role in the development of quantum physics and material science. Recently, the related researches have been extended to non-Hermitian regime [1], and evoked extreme repercussions [2–8]. However, some behaviors that are well-studied in Hermitian systems are challenged when moving to the NH field. For instance, for quite a long time, the bulk-boundary correspondence, which relates robust edge states to the bulk topological invariants, encounters difficulties [9–12]. Fortunately, with the establishment of generalized Brillouin zone (GBZ) theory, the problem is solved in some NH systems [2, 13]. It indicates that the usually used Brillouin zone (BZ) may break down in NH systems. Instead, the wave vector k may become complex, and the GBZ denotes the trajectory of the Bloch phase factor $\beta = e^{ik}$ in the complex plane. The establishment of GBZ theory makes it possible to predict the transition points and the existence of edge states in some of the NH systems, and also opens the gate for further studies.

One of the essential implementations of non-Hermiticity is through the open quantum system, among all the descriptions, the Lindblad Markov master equation is definitely the most reliable and accepted theory [14]. By solving the evolution of the density operator over time, it is possible to track the changes of the system's energy, information, coherence, etc. However, no matter studying the density operator or the corresponding Liouvillian operator [15], the calculation cost will be the square of the system Hilbert space dimension, which significantly increases the difficulty of the study. In most cases, only numerical solutions are available, especially for complicated many body systems. For these reasons, it is convenient to neglect the jumping terms in the master equation [4, 5, 16], because its effective NH Hamiltonian could provide a simpler description of dissipation. However, the quantum jumping terms may be non-negligible in many circumstances, because they could induce interesting phenomena or differences [15, 17]. From the point view of the wave function, the stochastic jumps may commit abrupt perturbation [18, 19], or influence the spectrum of Liouvillian operator

[15, 17, 20]. Given that both descriptions have established distinct theoretical frameworks, exploring their similarities and differences have drawn increasing attention in recent years [21–23]. Among them, the extension of topological phase in open quantum system is a particularly urgent task, but is still in its infancy [24–27]. Naturally, one may wonder how the quantum jumping terms would affect the topological properties. To answer this question, we will address the above issues and elucidate the effect of quantum jumps through a specific model.

In this paper, we mainly concentrate on the NH SSH model studied in Ref. [2], the difference is that the implementation of asymmetric hopping terms in the unit cell are through the Lindblad master equation with collective loss and gain. When all the jumping terms are ignored, they are dynamically equivalent. With the help of the third quantization technique as well as the GBZ theory, we deduce the shape matrix and study its topological properties. Compared with NH theory, the two approaches show high consistency in predicting transition points and topological edge states, which illustrates the validity of our scheme. Furthermore, we analyze the circumstances that the quantum jumping terms are involved, the transition points may be shifted and the break the original symmetry. It reveals that the quantum jump may have unique effect in topological systems, and should be carefully examined. Our work paves the way for defining the topological phase, which is a challenge of current researches.

This paper is organized as follows. In Sec. II we present the example model of the entire paper and introduce the basic theory of the third quantization. In Sec. III we classify the symmetries of the model in the presence of or absence of the jumping terms. In Sec. IV we apply the auxiliary GBZ theory to calculate the GBZ, and define the corresponding topological invariants in Sec. V, we also briefly discuss the preserving of bulk-boundary correspondence. Finally, in Sec. VI we conclude and dampen expectations.

II. MODEL

In this section, we start from a one-dimension SSH lattice [28] with dissipation, as shown in Fig. 1(a). The internal hopping strength between sites A and sites B is t_1 , and the hopping

* niuxy795@nenu.edu.cn

between the neighbor cells is t_2 . The Hamiltonian H of such model can be written as $H = \sum_n^{N/2} (t_1 c_{nA}^\dagger c_{nB} + t_2 c_{n+1A}^\dagger c_{nB} + \text{H.c.})$, where c is the annihilation operator of fermion and the subscript denotes the site A,B in the n th unit cell.

Considering the system is suffering loss and gain, it is convenient to be presented by the Lindblad master equation [14]

$$\mathcal{L}\rho = \dot{\rho} = -i[H, \rho] + \sum_\mu (2\kappa L_\mu \rho L_\mu^\dagger - \rho L_\mu^\dagger L_\mu - L_\mu^\dagger L_\mu \rho), \quad (1)$$

where \mathcal{L} is the Liouvillian superoperator. Terms $L_\mu \rho L_\mu^\dagger$ are usually called jumping terms, which represent the continuous measurements to the system induced by the environment. Here we add a real parameter κ , which characterizes the strength that the jump occurs, such structure is named as “hybrid Liouvillian” in Ref. [29]. In this work, we mainly focus on two common cases, the full dynamic of the master equation $\kappa = 1$ and the no jump case $\kappa = 0$. In recent works, the latter case could be achieved by considering specific short-time dynamic [30], performing post-selected operations [31] or assuming loss processes of a coherent condensate [32]. After the following procedures, they assume that the jumping terms in the master equation can be safely neglected, and the system is governed by an effective NH Hamiltonian

$$H_{eff} = H - \frac{i}{2} \sum_\mu L_\mu^\dagger L_\mu. \quad (2)$$

In our model, the Lindblad operators L_μ write

$$L_{1,n} = \sqrt{\gamma_l}(c_{nA} + i c_{nB}), \quad (3a)$$

$$L_{2,n} = \sqrt{\gamma_g}(c_{nA}^\dagger + i c_{nB}^\dagger), \quad (3b)$$

where $L_{1,n}$ stands for the collective one-body loss [32] and $L_{2,n}$ represents the gain, the γ_l, γ_g are the rates of loss and gain. These types of dissipation can also be found in Ref. [21, 33–35]. Without loss of generality, we assume $t_1, t_2, \gamma_l, \gamma_g$ are all real. When the jumping terms are absent ($\kappa = 0$), it is straightforward to find that the effective Hamiltonian H_{eff} in Eq. (2) takes

$$H_{eff} = \sum_n \left((t_1 + \frac{\gamma}{2}) c_{nA}^\dagger c_{nB} + (t_1 - \frac{\gamma}{2}) c_{nB}^\dagger c_{nA} + t_2 (c_{n+1A}^\dagger c_{nB} + c_{nB}^\dagger c_{n+1A}) - \frac{i}{2} \gamma' (c_{nA}^\dagger c_{nA} + c_{nB}^\dagger c_{nB}) \right), \quad (4)$$

here $\gamma = \gamma_l + \gamma_g$, $\gamma' = \gamma_l - \gamma_g$. Actually, the overall loss $-i\gamma'/2$ is negligible because $N = \sum_n (c_{nA}^\dagger c_{nA} + c_{nB}^\dagger c_{nB})$ is the total particle number of the system, which can be viewed as a constant [33]. Concisely, the properties of the system is completely determined by the effective model in Fig. 1(b). In Ref. [2], its GBZ and corresponding topological invariant is defined and calculated. The transition points can be faithfully predicted and the consistency between the edge states and winding number implies the establishment of new bulk-boundary correspondence in 1D non-Hermitian systems.

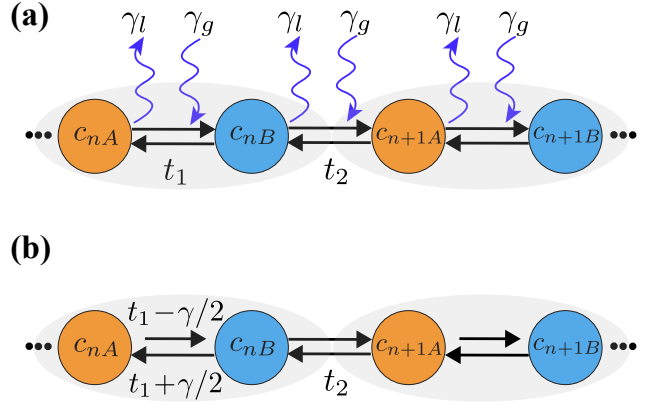


FIG. 1. (a) The SSH lattice with staggered hopping as well as loss and gain, the total number of sites is N . The intracell hopping strength is t_1 , the intercell hopping is t_2 , and the strength of collective loss and gain is γ_l and γ_g . When the quantum jump is absent, the dynamic is equivalent to (b), an effective NH SSH model with non-reciprocal hopping $t_1 \pm \gamma/2$, $\gamma = \gamma_l + \gamma_g$.

The third quantization

It is natural to ask, what may happen if the jumping terms $L_\mu \rho L_\mu^\dagger$ for any μ could not be neglected. However, this problem can become very difficult, since taking the jumping terms into consideration will lead to a rapid increase in matrix dimensionality $\propto N^2$ [15]. For such quadratic fermionic dissipative systems, by applying the third quantization approach established by Prosen *et al.* [36], the dimension could be reduced to $4N$, which will be useful for afterwards studies. We begin by transforming the model in terms of the *Majorana* operators

$$w_{2m-1} = c_m + c_m^\dagger, w_{2m} = i(c_m - c_m^\dagger), \quad (5)$$

where w_m satisfies the anticommutation relations $\{w_m, w_n\} = 2\delta_{mn}$. Under this basis, the free Hamiltonian H and Lindblad operators can be represented as $H = \sum_{jk} w_j H_{j,k} w_k$ and $L_\mu = \sum_\mu l_{\mu,j} w_j$. After mapping the Liouvillian operator \mathcal{L} into the Liouvillian-fork space [37, 38], we can define the creation and annihilation operators \hat{c}_j^\dagger and \hat{c}_j as (named as “a-fermions”, we use the “hat” for distinction)

$$\hat{c}_j |P_\alpha\rangle = \delta_{\alpha,j,1} |w_j P_\alpha\rangle, \hat{c}_j^\dagger |P_\alpha\rangle = \delta_{\alpha,j,0} |w_j P_\alpha\rangle, \alpha_j \in \{0, 1\}, \quad (6)$$

here the density matrix ρ is vectored to a linear combination of the 2^{2N} polynomials $P_\alpha = w_1^{\alpha_1} w_2^{\alpha_2} \dots w_{2N}^{\alpha_{2N}}$. The $|P_\alpha\rangle$ is the corresponding canonical basis of the vector space, and the inner product satisfies $\langle x|y\rangle = 4^{-N} \text{tr} x^\dagger y$.

By using Eq. (1),(6), after some mathematical calculations, we can obtain the each part of the Lindblad maps. The Liouvillian \mathcal{L} can be split into $\mathcal{L} = \mathcal{L}_0 + \mathcal{L}_{diss}$, the first part $\mathcal{L}_0 \rho := -i[H, \rho]$ describes the unitary evolution, which is governed by the free Hamiltonian H and its a-Fermi maps write

$$\hat{\mathcal{L}}_0 = -4i \sum_{j,k} \hat{c}_j^\dagger H_{j,k} \hat{c}_k, \quad (7)$$

the second part $\mathcal{L}_{diss}\rho := \mathcal{L}_{eff}\rho + \kappa\mathcal{L}_{jump}\rho = \sum_{\mu}(2\kappa L_{\mu}\rho L_{\mu}^{\dagger} - \rho L_{\mu}^{\dagger}L_{\mu} - L_{\mu}^{\dagger}L_{\mu}\rho)$ represents the dissipation. In order to quantify the effect of quantum jumps, we divided \mathcal{L}_{diss} into \mathcal{L}_{eff} and \mathcal{L}_{jump} , which is induced by the effective theory and jumping terms, respectively

$$\hat{\mathcal{L}}_{eff} = \sum_{j,k,\mu} 2l_{\mu,j}l_{\mu,k}^*(\hat{c}_j^{\dagger}\hat{c}_k^{\dagger} + \hat{c}_j\hat{c}_k), \quad (8)$$

$$\hat{\mathcal{L}}_{jump} = \sum_{j,k,\mu} 2l_{\mu,j}l_{\mu,k}^*e^{i\pi\hat{N}}(\hat{c}_j^{\dagger}\hat{c}_k^{\dagger} - \hat{c}_j^{\dagger}\hat{c}_k - \hat{c}_k^{\dagger}\hat{c}_j - \hat{c}_j\hat{c}_k), \quad (9)$$

where $\hat{N} = \sum_j \hat{c}_j^{\dagger}\hat{c}_j$ is the total number of “a-fermions”. In the even parity subspace Eq. (9) becomes [36]

$$\hat{\mathcal{L}}_{jump} = \sum_{j,k,\mu} 2l_{\mu,j}l_{\mu,k}^*(\hat{c}_j^{\dagger}\hat{c}_k^{\dagger} - \hat{c}_j^{\dagger}\hat{c}_k - \hat{c}_k^{\dagger}\hat{c}_j - \hat{c}_j\hat{c}_k). \quad (10)$$

When considering the full dynamic ($\kappa = 1$), by using Eq. (8),(10), $\hat{\mathcal{L}}_{diss}$ takes

$$\hat{\mathcal{L}}_{diss} = \sum_{j,k,\mu} l_{\mu,j}l_{\mu,k}^*(4\hat{c}_j^{\dagger}\hat{c}_k^{\dagger} - 2\hat{c}_j^{\dagger}\hat{c}_k - 2\hat{c}_k^{\dagger}\hat{c}_j). \quad (11)$$

After linearization by *adjoint Hermitian Majorana maps* [36], the dissipative system is decomposed into normal master modes (NMMs), $\hat{a}_{2j-1} = 1/\sqrt{2}(\hat{c}_j + \hat{c}_j^{\dagger})$, $\hat{a}_{2j} = i/\sqrt{2}(\hat{c}_j - \hat{c}_j^{\dagger})$, the Liouvillian can be written as

$$\hat{\mathcal{L}} = \sum_{j,k}^{4n} \hat{a}_j \mathbf{A} \hat{a}_k, \quad (12)$$

where the \mathbf{A} is usually named as *shape matrix*, whose elements satisfy

$$\mathbf{A}_{2j-1,2k-1} = -2iH_{jk} - \sum_{\mu} l_{\mu,j}l_{\mu,k}^* + \sum_{\mu} l_{\mu,k}l_{\mu,j}^*, \quad (13a)$$

$$\mathbf{A}_{2j-1,2k} = -2H_{jk} + 2i \sum_{\mu} l_{\mu,k}l_{\mu,j}^*, \quad (13b)$$

$$\mathbf{A}_{2j,2k-1} = 2H_{jk} - 2i \sum_{\mu} l_{\mu,j}l_{\mu,k}^*, \quad (13c)$$

$$\mathbf{A}_{2j,2k} = -2iH_{jk} + \sum_{\mu} l_{\mu,j}l_{\mu,k}^* - \sum_{\mu} l_{\mu,k}l_{\mu,j}^*. \quad (13d)$$

The shape matrix of the model

By applying Eq. (7),(8),(10) to our model (Fig.1(a)), the shape matrix \mathbf{A} is written as the sum of unitary part \mathbf{A}_0 and dissipation part \mathbf{A}_{diss} , $\mathbf{A} = \mathbf{A}_0 + \mathbf{A}_{diss}$, the banded form writes

$$\mathbf{A}_0 = \begin{pmatrix} & t_1 T & & & t_2 T \\ t_1 T & & t_2 T & & \\ & t_2 T & & t_1 T & \\ & & \ddots & & \ddots \\ t_2 T & & & & \end{pmatrix}, \quad (14)$$

here $T = -i\sigma_y \otimes I_2$, where σ_y is the pauli matrix and I_2 is the identity operator. Here, for the sake of simplicity, we only consider the special case when there is only loss in the dissipation term \mathbf{A}_{diss} (the loss and gain case will be discussed afterwards)

$$\mathbf{A}_{diss} = \begin{pmatrix} A & B & & & \\ -B & A & & & \\ & & A & B & \\ & & & \ddots & \ddots \\ & & & & -B & A \end{pmatrix}, \quad (15)$$

where the A and B can be calculated through Eq. (3a),(8),(10) with

$$A = -\frac{\gamma_l}{2} \begin{pmatrix} 0 & -i\kappa & -i & \kappa \\ i\kappa & 0 & \kappa & i \\ i & -\kappa & 0 & -i\kappa \\ -\kappa & -i & i\kappa & 0 \end{pmatrix}, B = -\frac{\gamma_l}{2} \begin{pmatrix} i & -\kappa & 0 & -i\kappa \\ -\kappa & -i & i\kappa & 0 \\ 0 & i\kappa & i & -\kappa \\ -i\kappa & 0 & -\kappa & -i \end{pmatrix}. \quad (16)$$

Suppose the model is under period boundary condition (PBC), it is relatively simple to transform into the momentum space, with the Fourier transform, the Bloch shape matrix writes

$$\mathbf{A}(k) = \begin{pmatrix} A & (t_1 + t_2 e^{-ik})T + B \\ (t_1 + t_2 e^{ik})T - B & A \end{pmatrix}. \quad (17)$$

On the other side, when the jumping terms are absent ($\kappa = 0$), the shape matrix $\mathbf{A}' = \mathbf{A}_0 + \mathbf{A}'_{diss}$ takes

$$\mathbf{A}' = -\frac{\gamma_l}{2} \begin{pmatrix} 0 & 0 & -i & 0 \\ 0 & 0 & 0 & i \\ i & 0 & 0 & 0 \\ 0 & -i & 0 & 0 \end{pmatrix}, \mathbf{B}' = -\frac{\gamma_l}{2} \begin{pmatrix} i & 0 & 0 & 0 \\ 0 & -i & 0 & 0 \\ 0 & 0 & i & 0 \\ 0 & 0 & 0 & -i \end{pmatrix}. \quad (18)$$

Similarly, by using Eq. (8),(10), the Bloch form shape matrix $\mathbf{A}'(k)$ is the same as Eq. (17), except that A, B are substituted by A', B'

$$\mathbf{A}'(k) = \begin{pmatrix} A' & (t_1 + t_2 e^{-ik})T + B' \\ (t_1 + t_2 e^{ik})T - B' & A' \end{pmatrix}. \quad (19)$$

It is worth stressing that the diagonal block A' in Eq. (19) can be discarded, because it represents the overall loss (correspond to the last term in Eq. (4)), and the Liouvillian \mathcal{L} will remain unchanged after such gauge shift $H \rightarrow H + cI$, where I is the identity operator and c is a complex c-number [39].

By using Eq. (14)-(19), we can find that \mathbf{A}, \mathbf{A}' have the same set of eigenvalues $\lambda \in \{E_{\mu}\}$ (where the eigenvalues with positive real parts are referred to as “rapidities” [36]. Here we use the label μ to represent different bands (or solutions))

$$E_{1,\pm}(\beta) = \gamma/2 \pm \sqrt{(\gamma/2 + t_1 + t_2\beta)(\gamma/2 - t_1 - t_2\beta)}, \\ E_{2,\pm}(\beta) = -\gamma/2 \pm \sqrt{(\gamma/2 + t_1 + t_2\beta)(\gamma/2 - t_1 - t_2\beta)}, \quad (20)$$

which remains unchanged for arbitrary value of the jump parameter κ , here we use the notation $e^{ik} = \beta$.

III. SYMMETRY

The characterization of topology is closely associated with its symmetry. For noninteracting fermions, the topological classification can be sorted into the Altland-Zirnbauer (AZ) symmetry class [40–42]. Based on the presence or absence of the three basic symmetries, time-reversal symmetry (TRS), particle-hole symmetry (PHS) and chiral symmetry (or sublattice symmetry), that is

$$\text{TRS}: H = U_T H^* U_T^\dagger, U_T U_T^* = \pm I, \quad (21a)$$

$$\text{PHS}: H = -U_C H^* U_C^\dagger, U_C U_C^* = \pm I, \quad (21b)$$

$$\text{chiral}: H = -U_S H U_S^\dagger, U_S^2 = I, \quad (21c)$$

their combinations will process a ten-fold classification as shown in Appendix A. Here U_T, U_C, U_S are all unitary matrices, corresponding to the TRS, PHS and chiral symmetry, respectively. Intriguingly, although the introduction of non-Hermiticity will enrich the topological phases into a 38-fold classification [43], it has been proved that the symmetries for quadratic Lindbladians with linear Lindblad operators may still preserve the tenfold way [44, 45].

Precisely, by using pauli matrix, we can rewrite Eq. (17) as

$$\begin{aligned} \mathbf{A}(k) = & -i(t_1 + t_2 \cos k) \sigma_x \otimes (\sigma_y \otimes I_2) - it_2 \sin k \sigma_y \otimes \\ & (\sigma_y \otimes I_2) - \frac{i\gamma}{2} \sigma_y \otimes (I_2 \otimes (i\sigma_z - \kappa \sigma_x) + i\kappa \sigma_y \otimes \sigma_y) - \frac{\gamma}{2} \kappa I_2 \\ & \otimes I_2 \otimes \sigma_y + \frac{i\gamma}{2} I_2 \otimes \sigma_y \otimes (i\sigma_z - \kappa \sigma_x), \end{aligned} \quad (22)$$

when there is no jump and the overall loss is neglected, Eq. (19) becomes

$$\begin{aligned} \mathbf{A}'(k) = & -i(t_1 + t_2 \cos k) \sigma_x \otimes (\sigma_y \otimes I_2) - it_2 \sin k \sigma_y \otimes \\ & (\sigma_y \otimes I_2) + \frac{\gamma}{2} \sigma_y \otimes I_2 \otimes \sigma_z. \end{aligned} \quad (23)$$

Obviously, it is easy to prove that Eq. (22) fulfills TRS in Eq. (21b), and $U_T U_T^* = -I$

$$U_T \mathbf{A}'(k) U_T^{-1} = \mathbf{A}(-k), \quad (24)$$

where $U_T = I_2 \otimes \sigma_y \otimes \sigma_x$. On the other hand, Eq. (23) satisfies chiral symmetry in Eq. (21c)

$$\mathbf{A}'(k) = U_S \mathbf{A}'(k) U_S^{-1}, \quad (25)$$

and $S = \sigma_z \otimes I_2 \otimes I_2$. Meanwhile $\mathbf{A}'(k)$ also has other symmetries (TRS in Eq. (21a) and PHS in Eq. (21b))

$$\mathbf{A}'(k) = U_T \mathbf{A}'(-k) U_T^{-1}, \quad (26)$$

$$\mathbf{A}'(k) = -U_C \mathbf{A}'(-k) U_C^{-1}, \quad (27)$$

where $U_T = I_2 \otimes \sigma_y \otimes \sigma_x$ and $U_C = \sigma_z \otimes \sigma_y \otimes \sigma_x$. By applying the classification method in Appendix A, the entire classification of Eq. (22) is of Class CII. The presence of jumping terms will break PHS and chiral symmetry, and yields an AII class.

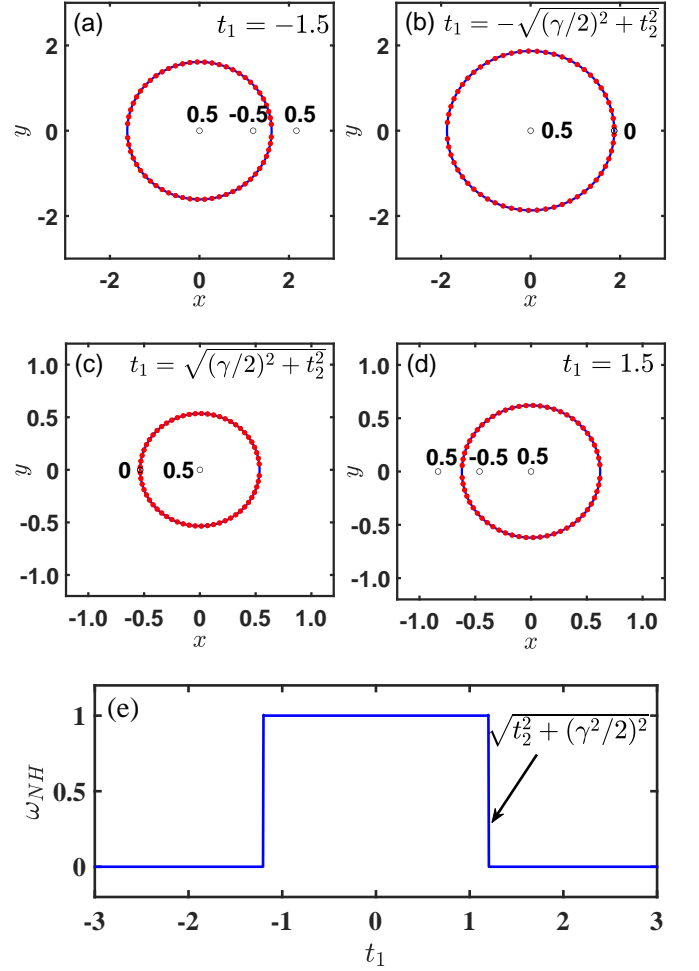


FIG. 2. (a-d) The GBZ of the effective model (Fig. 1(b)), poles (black circles) and the corresponding residues of the winding number in Eq. (45). The blue solid lines represent the GBZ obtained by aGBZ theory, whereas the red points are the numerical results of Eq. (33) ($N = 60$). The parameters are chosen as (a) $t_1 = -1.5$, (b) $t_1 = -\sqrt{(\gamma/2)^2 + t_2^2} \approx -1.2019$, (c) $t_1 = \sqrt{(\gamma/2)^2 + t_2^2} \approx 1.2019$, (d) $t_1 = 1.5$. The 0 residues in (b),(c) are the second order poles, while others are of the first order. (e) The topological invariant as a function of t_1 , the transition points are at $t_1 = \pm \sqrt{(\gamma/2)^2 + t_2^2}$. In (a-e) we have $t_2 = 1, \gamma = 4/3$.

IV. GENERALIZED BRILLOUIN ZONE

As a central principle of Hermitian topological systems, the bulk-edge correspondence has always been extensively investigated. It reveals that the number of the edge states under open boundary condition (OBC) can be faithfully predicted by the topological invariant under PBC. Nevertheless, its promotion to non-Hermitian systems is still a pending issue, even the simplest NH models are controversially debated and discussed. For example, researchers have considered introducing fractional winding numbers to modify the previous conclusions [6, 10]. However, it is argued by Ref. [2, 11] because

the topological winding number defined in this manner fails to predict the phase transition points. Comparatively, as a generalization of conventional BZ, their GBZ theory reveals that the wave number k in Hermitian cases is now complex in non-Hermitian systems, and instead, the real and imaginary parts of the phase factor in Bloch waves $\beta = e^{ik}$ is generally no longer a unit circle (see Appendix B for more details). Besides, in some NH systems, the wave function may not spread across the bulk, but localizes at the boundary (dubbed the “Non-Hermitian skin effect”) [46]. Though there are still some works that present different insights [9, 47], the GBZ theory sparks a wave of researches on topological non-Hermitian systems [48–51].

Resultant

To obtain the information of the GBZ, the numerical solutions of the OBC spectrum shall be calculated first, which is the intrinsic requirement of the eigen-function Eq. (B4). However, in practice the contours of GBZ are sensitive to the dimension and calculation precision. The inappropriate value selection may cause unpredictable errors, or unacceptable calculation time. To avoid these problems, we use a kind of analytic calculation method introduced in Ref. [52], where the authors use a mathematical technique called *Resultant* to deal with these equations, suppose there are two polynomials $f(x) = a_n x^n + \dots + a_0 = \prod_{i=1}^n (x - \xi_i)$, $g(x) = b_m x^m + \dots + b_0 = \prod_{j=1}^m (x - \eta_j)$ which respect to x , their *Resultant* is defined as

$$R_x(f, g) = a_n^m b_m^n \prod_{i,j} (\xi_i - \eta_j). \quad (28)$$

In Mathematics, the *Resultant* can be used to eliminate variables in the polynomial, and obtain the expression which only relies on other variables. Precisely, suppose there are two polynomials function $f(x, y)$, $g(x, y) = 0$, where f, g is a function of both x and y , to fully remove the effect of x , and only remains the variable y , the relationship satisfies

$$R_x[f(x, y), g(x, y)] = 0, \quad (29)$$

this property can help us to obtain the GBZ of the system, and will be discussed later.

The calculation of aGBZ

From Appendix B, we have known that $f(\beta, E) = 0$ and there shall have at least a pair of solutions β which has the same norm $|\beta_M| = |\beta_{M+1}|$, thus we can assume $\beta_M = \beta_0$ and $\beta_{M+1} = \beta_0 e^{i\theta}$, where β_0 is a complex number, so that the following relationship holds

$$f(\beta_0, E) = f(\beta_0 e^{i\theta}, E) = 0, \theta \in \mathcal{R}. \quad (30)$$

By using the property of *Resultant* in Eq. (29), it is easy to eliminate E in Eq. (30), and yields

$$G(\beta, \theta) = R_E(f(\beta, E), f(\beta e^{i\theta}, E)) = 0. \quad (31)$$

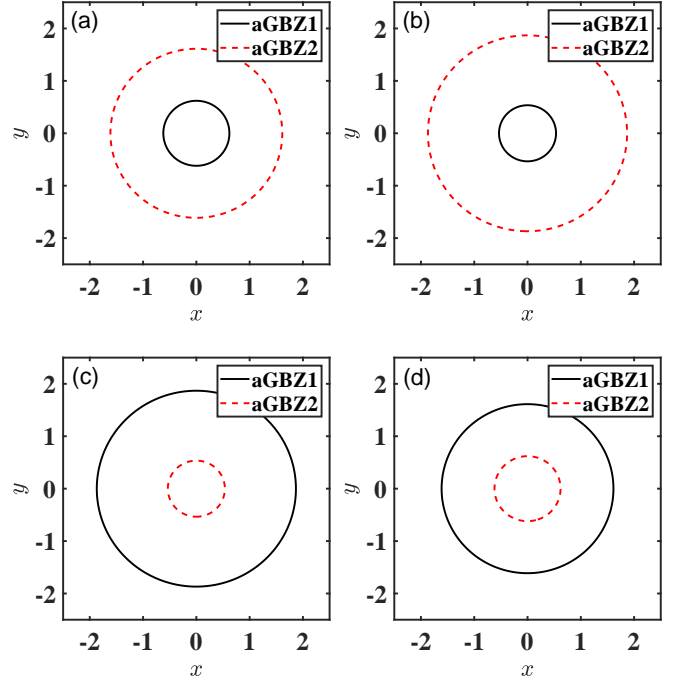


FIG. 3. The aGBZ of open quantum description (Eq. (19)) without quantum jump. The black solid and red dashed line are arcs of aGBZ in Eq. (37b),(38a). The same as Fig. 2(a)-2(d), parameters are chosen as (a) $t_1 = -1.5$, (b) $t_1 = -\sqrt{(\gamma/2)^2 + t_2^2}$, (c) $t_1 = \sqrt{(\gamma/2)^2 + t_2^2}$, (d) $t_1 = 1.5$, and $t_2 = 1$, $\gamma = 4/3$.

Obviously it requires both real and imaginary parts of $G(\beta, \theta)$ to be zero, $\text{Re}[G(\beta, \theta)] = 0, \text{Im}[G(\beta, \theta)] = 0$. The next step is to eliminate the variable θ , by using Weierstrass substitution, $\cos \theta = (1 - t^2)/(1 + t^2)$, $\sin \theta = 2t/(1 + t^2)$, to substitute the parameter θ , we will obtain

$$R_t[\text{Re}(G(\beta, \theta)), \text{Im}(G(\beta, \theta))] = 0. \quad (32)$$

After the above treatments, both the variables E and θ will not appear anymore. By decomposing the resultant in Eq. (32), the nontrivial results outline the curves of auxiliary generalized Brillouin zone (aGBZ). In general, the actual GBZ is usually a subset of aGBZ [52].

The GBZ of the effective NH Hamiltonian

In this section, we first consider the GBZ of the effective non-Hermitian Eq. (4), and for the sake of simplicity, we take $\gamma_g = 0$ and $\gamma_l = \gamma$ in Eq. (3a),(3b). Thus the model will be simplified to the case discussed in Ref. [2]

$$\left[\left(t_1 - \frac{\gamma}{2} \right) + t_2 \beta \right] \left[\left(t_1 + \frac{\gamma}{2} \right) + t_2 \beta^{-1} \right] = E^2, \quad (33)$$

here E is the energy of bulk-band in OBC, and β is obtained by using Eq. (B7). By using the technique in the previous subsection, we can substitute Eq. (33) into Eq. (31) and (32),

and obtain the constraint equations of GBZ

$$\frac{\gamma}{2} - t_1 + (\frac{\gamma}{2} + t_1)(x^2 + y^2) = 0, \quad (34a)$$

$$-\frac{\gamma}{2} + t_1 + (\frac{\gamma}{2} + t_1)(x^2 + y^2) = 0, \quad (34b)$$

here $x = \text{Re}\beta$ and $y = \text{Im}\beta$, which describe the trajectory of β . In Fig. 2(a)-2(d) we display the GBZ of the effective model, calculated by the method of aGBZ (blue solid line), and Eq. (33) (scattered red dots), respectively. Apparently the two results are consistent, except that the trajectory becomes extremely loose near the real axis, while the aGBZ so-

lution can give an explicit closed region. The aGBZ scheme is more recommended to use, which is especially evident in some complicated systems.

The aGBZ of shape matrix when no jump

Next we will turn to open quantum description, we first consider the case in the absence of the jumping terms (Eq. (19), and the overall loss is neglected), whose dynamic is the same as the effective non-Hermitian (Eq. (4)). By analogy, the eigen-function of \mathbf{A} at the bulk writes

$$\begin{pmatrix} 0 & 0 & -t_2 & 0 & 0 & 0 & 0 & 0 & -\frac{i\gamma}{2} & 0 & -t_1 & 0 & 0 & 0 & 0 & 0 \\ 0 & 0 & 0 & -t_2 & 0 & 0 & 0 & 0 & 0 & \frac{i\gamma}{2} & 0 & -t_1 & 0 & 0 & 0 & 0 \\ t_2 & 0 & 0 & 0 & 0 & 0 & 0 & 0 & 0 & t_1 & 0 & -\frac{i\gamma}{2} & 0 & 0 & 0 & 0 \\ 0 & t_2 & 0 & 0 & 0 & 0 & 0 & 0 & 0 & 0 & t_1 & 0 & \frac{i\gamma}{2} & 0 & 0 & 0 \\ 0 & 0 & 0 & 0 & \frac{i\gamma}{2} & 0 & -t_1 & 0 & 0 & 0 & 0 & 0 & 0 & 0 & -t_2 & 0 \\ 0 & 0 & 0 & 0 & 0 & -\frac{i\gamma}{2} & 0 & -t_1 & 0 & 0 & 0 & 0 & 0 & 0 & 0 & -t_2 \\ 0 & 0 & 0 & 0 & t_1 & 0 & \frac{i\gamma}{2} & 0 & 0 & 0 & 0 & 0 & t_2 & 0 & 0 & 0 \\ 0 & 0 & 0 & 0 & 0 & 0 & t_1 & 0 & -\frac{i\gamma}{2} & 0 & 0 & 0 & 0 & t_2 & 0 & 0 \end{pmatrix} \begin{pmatrix} \psi_{nA1} \\ \psi_{nA2} \\ \psi_{nA3} \\ \psi_{nA4} \\ \psi_{nB1} \\ \psi_{nB2} \\ \psi_{nB3} \\ \psi_{nB4} \\ \psi_{n+1A1} \\ \psi_{n+1A2} \\ \psi_{n+1A3} \\ \psi_{n+1A4} \\ \psi_{n+1B1} \\ \psi_{n+1B2} \\ \psi_{n+1B3} \\ \psi_{n+1B4} \end{pmatrix} = E \begin{pmatrix} \psi_{nA1} \\ \psi_{nA2} \\ \psi_{nA3} \\ \psi_{nA4} \\ \psi_{nB1} \\ \psi_{nB2} \\ \psi_{nB3} \\ \psi_{nB4} \end{pmatrix}, \quad (35)$$

where the eigenvectors of the shape matrix can be written as $|\Psi\rangle = (\psi_{1A1}, \psi_{1A2}, \psi_{1A3}, \psi_{1A4}, \psi_{1B1}, \psi_{1B2}, \psi_{1B3}, \psi_{1B4}, \dots)^T$, where $\psi_{m\sigma n}$ is the wave function at site $\sigma = A, B$, and m is the index of the cell, $n = 1, 2, 3, 4$ stands for the NMM bands in Eq. (5).

After using the characteristic equation in Eq. (B3),(B4), in order to have non-zero solutions, the determinant of the coefficient matrix shall equal to zero, which indicates

$$E^2 - \gamma^2/4 + t_1^2 + \frac{\gamma t_2}{2\beta} - \frac{\beta \gamma t_2}{2} + \frac{t_1 t_2}{\beta} + \beta t_1 t_2 + t_2^2 = 0, \quad (36a)$$

$$E^2 - \gamma^2/4 + t_1^2 - \frac{\gamma t_2}{2\beta} + \frac{\beta \gamma t_2}{2} + \frac{t_1 t_2}{\beta} + \beta t_1 t_2 + t_2^2 = 0, \quad (36b)$$

by substituting Eq. (36a),(36b) into Eq. (31),(32) to eliminate the addition degrees E, θ , the irreducible factors of $R_t[\text{Re}(G), \text{Im}(G)] = 0$ present the trajectory of aGBZ. Eq. (36a) indicates

$$-\gamma/2 - t_1 + (\gamma/2 - t_1)(x^2 + y^2) = 0, \quad (37a)$$

$$\text{or } \gamma/2 + t_1 + (\gamma/2 - t_1)(x^2 + y^2) = 0, \quad (37b)$$

while Eq. (36b) shows

$$\gamma/2 - t_1 + (\gamma/2 + t_1)(x^2 + y^2) = 0, \quad (38a)$$

$$\text{or } -\gamma/2 + t_1 + (\gamma/2 + t_1)(x^2 + y^2) = 0, \quad (38b)$$

same as previous, x, y takes $x = \text{Re}\beta$ and $y = \text{Im}\beta$.

In Fig. 3(a)-3(d) we depict the curves of aGBZ plotted under different sets of parameters, each of which possesses two closed loops. Such circumstance is general for multiband systems, because different factorizations $E_\mu(\beta)$ of the characteristic equation in Eq. (B4) may lead to distinct sub-GBZ bands (Eq. (B5)). In order to obtain GBZ from aGBZ, an inspection is required to prevent extraneous roots. The reason is that we eliminate the variable E in Eq. (31), however, the continuous band spectrum of OBC is bounded, which means all possible values in the complex plane could be taken. In Appendix C, we briefly introduce the definition of self-conjugate points in aGBZ, which will allow us to accurately determine the actual area of the GBZ, any analytic arc that contains these points must form GBZ [52].

Applying the above conclusions, in Fig. 4(a)-4(d), we show the self-conjugate points β_0 as well as the corresponding end points E_0 of the OBC spectrum with cyan marks by solving Eq. (C4), we chose $t_1 = \sqrt{(\gamma/2)^2 + t_2^2} \pm 0.05$, which is close

to the transition points. The critical points pass through the curves of both aGBZ, thus the two branches of the closed loop in Fig. 3(a)-3(d) are either aGBZ or GBZ.

The GBZ of shape matrix when jump presented

In order to visualize the effect of jumping terms, in this subsection, we use the above methods for the case that quantum jumps are involved. By substituting Eq. (14),(15) into Eq. (B3), the eigen-function reads

$$\begin{pmatrix} \frac{i\gamma}{2} & -\frac{\gamma}{2}\kappa & -t_1 & -\frac{i\gamma}{2}\kappa & 0 & \frac{i\gamma}{2}\kappa & \frac{i\gamma}{2} & -\frac{\gamma}{2}\kappa & 0 & 0 & -t_2 & 0 & 0 & 0 & 0 & 0 \\ -\frac{\gamma}{2}\kappa & -\frac{i\gamma}{2} & \frac{i\gamma}{2}\kappa & -t_1 & -\frac{i\gamma}{2}\kappa & 0 & -\frac{\gamma}{2}\kappa & -\frac{i\gamma}{2} & 0 & 0 & 0 & -t_1 & 0 & 0 & 0 & 0 \\ t_1 & \frac{i\gamma}{2}\kappa & \frac{i\gamma}{2} & -\frac{\gamma}{2}\kappa & -\frac{i\gamma}{2}\kappa & \frac{\gamma}{2}\kappa & 0 & \frac{i\gamma}{2}\kappa & t_2 & 0 & 0 & 0 & 0 & 0 & 0 & 0 \\ -\frac{i\gamma}{2}\kappa & t_1 & -\frac{\gamma}{2}\kappa & -\frac{i\gamma}{2} & \frac{\gamma}{2}\kappa & \frac{i\gamma}{2} & -\frac{i\gamma}{2}\kappa & 0 & 0 & t_2 & 0 & 0 & 0 & 0 & 0 & 0 \\ 0 & 0 & 0 & 0 & 0 & 0 & -t_2 & 0 & 0 & \frac{i\gamma}{2}\kappa & \frac{i\gamma}{2} & -\frac{\gamma}{2}\kappa & -\frac{i\gamma}{2} & \frac{\gamma}{2}\kappa & -t_1 & \frac{i\gamma}{2}\kappa \\ 0 & 0 & 0 & 0 & 0 & 0 & 0 & -t_2 & -\frac{i\gamma}{2}\kappa & 0 & -\frac{\gamma}{2}\kappa & -\frac{i\gamma}{2} & \frac{\gamma}{2}\kappa & -\frac{i\gamma}{2} & -t_1 & -\frac{i\gamma}{2}\kappa \\ 0 & 0 & 0 & 0 & t_2 & 0 & 0 & 0 & -\frac{i\gamma}{2}\kappa & \frac{\gamma}{2}\kappa & 0 & \frac{i\gamma}{2}\kappa & t_1 & -\frac{i\gamma}{2}\kappa & -\frac{\gamma}{2}\kappa & \frac{\gamma}{2}\kappa \\ 0 & 0 & 0 & 0 & 0 & t_2 & 0 & 0 & \frac{\gamma}{2}\kappa & \frac{i\gamma}{2} & -\frac{i\gamma}{2}\kappa & 0 & \frac{i\gamma}{2}\kappa & t_1 & \frac{\gamma}{2}\kappa & \frac{i\gamma}{2} \end{pmatrix} \begin{pmatrix} \psi_{nA1} \\ \psi_{nA2} \\ \psi_{nA3} \\ \psi_{nA4} \\ \psi_{nB1} \\ \psi_{nB2} \\ \psi_{nB3} \\ \psi_{nB4} \\ \psi_{n+1A1} \\ \psi_{n+1A2} \\ \psi_{n+1A3} \\ \psi_{n+1A4} \\ \psi_{n+1B1} \\ \psi_{n+1B2} \\ \psi_{n+1B3} \\ \psi_{n+1B4} \end{pmatrix} = E \begin{pmatrix} \psi_{nA1} \\ \psi_{nA2} \\ \psi_{nA3} \\ \psi_{nA4} \\ \psi_{nB1} \\ \psi_{nB2} \\ \psi_{nB3} \\ \psi_{nB4} \end{pmatrix}, \quad (39)$$

following similar procedures, we will have

$$E^2 - \gamma E + \frac{\gamma t_2}{2\beta} - \frac{\gamma t_2}{2}\beta + \frac{t_1 t_2}{\beta} + \beta t_1 t_2 + t_1^2 + t_2^2 = 0, \quad (40a)$$

$$E^2 + \gamma E - \frac{\gamma t_2}{2\beta} + \frac{\gamma t_2}{2}\beta + \frac{t_1 t_2}{\beta} + \beta t_1 t_2 + t_1^2 + t_2^2 = 0, \quad (40b)$$

which is independent of the quantum-jump parameter κ . Meanwhile, it also indicates that the corresponding GBZ region remains unchanged. When $\kappa = 0$ and the overall loss is neglected, we will return to the no jump case in the previous subsection.

V. TOPOLOGICAL INVARIANTS WITH OR WITHOUT QUANTUM JUMP

In Sec. III, we have known that when there is no jump, the shape matrix \mathbf{A}' (Eq. (19)) follows chiral symmetry. Invariants with such type of classification are usually defined by the “Q” matrix approach [53]. By choosing a proper basis that makes the symmetry operator diagonal, the Hamiltonian H can be written as

$$H = \begin{pmatrix} & h_+ \\ h_- & \end{pmatrix}, \quad (41)$$

where h_{\pm} is a matrix and for Hermitian cases $h_- = h_+^*$. For a non-Hermitian system, the special internal symmetry may determine a relationship between h_+ and h_- [33]. The eigen-

vectors and eigenvalues of H satisfy [13]

$$h_+ h_- |\psi_{\mu}^R\rangle = E_{\mu}^2(\beta) |\psi_{\mu}^R\rangle, \quad (42)$$

where the $|\psi_{\mu}^R\rangle, |\psi_{\mu}^L\rangle$ are the right and left eigenvectors of $h_+ h_-$ and $\langle \psi_{\nu}^L | \psi_{\mu}^R \rangle = \delta_{\mu,\nu}$. Hence the Q matrix can be defined as

$$Q = \begin{pmatrix} q^{-1}(\beta) & q(\beta) \end{pmatrix}, \quad (43)$$

where $q(\beta) = \sum_{\mu} q_{\mu}(\beta) = \sum_{\mu} \frac{1}{E_{\mu}(\beta)} |\psi_{R,\mu}(\beta)\rangle \langle \psi_{L,\mu}(\beta)| h_+$. The total winding number can be defined via the Q matrix, for single GBZ models [54]

$$\omega_{\mu} = \frac{1}{2\pi i} \oint_{\beta_{GBZ}} \text{Tr}[q(\beta)^{-1} dq(\beta)] = \frac{1}{2\pi i} \oint_{\beta_{GBZ}} d \ln \det [q(\beta)], \quad (44)$$

where the β_{GBZ} is the GBZ of the model.

For the effective Hamiltonian we consider in Eq. (4), according to Eq. (44), it is easy to know that $h_+ = t_1 + t_2/\beta + \gamma/2$, $h_- = t_1 + t_2\beta - \gamma/2$, and the total winding number will become

$$\omega_{NH} = \frac{1}{2\pi i} \oint_{\beta_{NH}} \left(\frac{t_2}{2\beta(\beta(\gamma/2 + t_1) + t_2)} - \frac{t_2}{2(\gamma/2 - (t_1 + \beta t_2))} \right) d\beta, \quad (45)$$

the GBZ region β_{NH} is depicted by Eq. (34a),(34b). In Fig. 2(e), we plot the chiral winding number calculated by Eq. (45) as a function of t_1 .

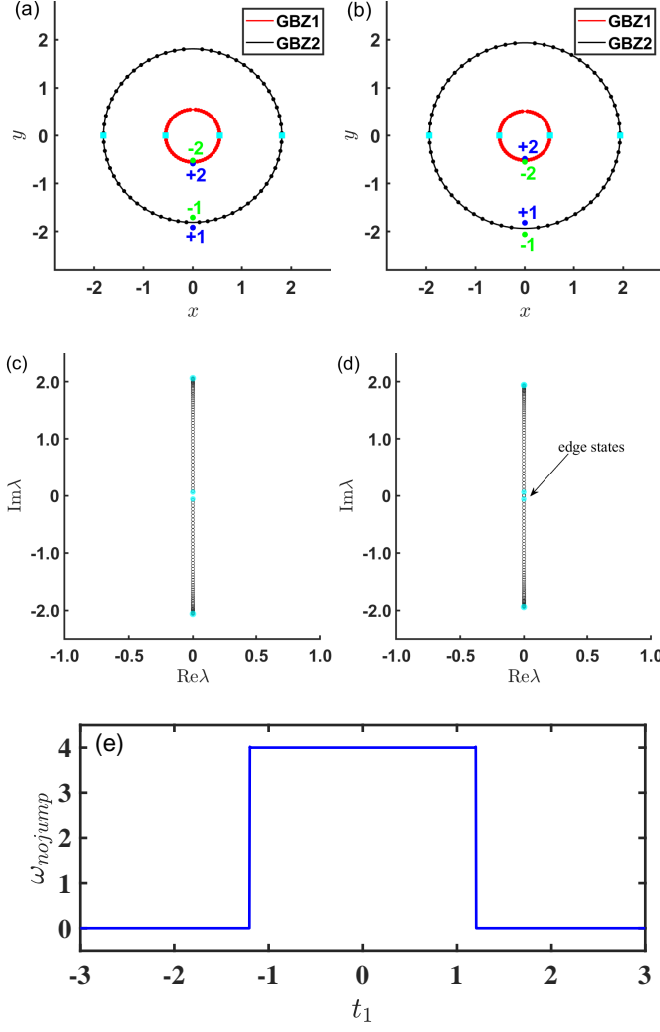


FIG. 4. (a-b) The sub-GBZs of the model in the absence of quantum jump. In (a)-(b), the red or blue arcs, scattered dots, and blue (green) points represent the aGBZ, numerical results ($N = 60$) and zeros of $\det(h_1)$ ($\det(h_2)$). (c-d) The spectrum of A' (black circles, $N = 50$). The self-conjugate points ($\beta_M = \beta_{M+1}$) are labeled in (a-d) with cyan marks, which indicate the model have multiple GBZ. The parameters are chosen to be $t_2 = 1, \gamma = 4/3$, (a,c) $t_1 = \sqrt{(\gamma/2)^2 + t_2^2} + 0.05 \approx 1.2519$, and (b,d) $t_1 = \sqrt{(\gamma/2)^2 + t_2^2} - 0.05 \approx 1.1519$. It is obviously that there is zero eigen-energy in (d) (eightfold degenerate). (e) The winding number calculated by Eq. (49).

In the same fashion, from Eq. (22), it directly implies

$$\begin{aligned} h_+ &= -i(t_1 + t_2 \cos k)(\sigma_y \otimes I_2) - t_2 \sin k(\sigma_y \otimes I_2) - i\gamma I_2 \otimes \sigma_z, \\ h_- &= -i(t_1 + t_2 \cos k)(\sigma_y \otimes I_2) + t_2 \sin k(\sigma_y \otimes I_2) + i\gamma I_2 \otimes \sigma_z. \end{aligned} \quad (46)$$

In this case, calculating the winding number of the system will be a bit complicated, since we will face the problem of integration over multiple sub-GBZs. Based on intuition, we shall combine Eq. (41),(44),(46), and write the total winding

number as a sum over all GBZ bands $\beta_{GBZ,\mu}$

$$\omega_{nojump} = \frac{1}{2\pi i} \sum_{\mu} \oint_{\beta_{GBZ,\mu}} \text{Tr}[q_{\mu}^{-1} \partial_{\beta} q_{\mu}], \quad (47)$$

where the region of $\beta_{GBZ,1,2}$ is given by Eq. (37a)- Eq. (38b). However, this is not the case in reality, because the sum of the winding number of each band $E_{\mu}(\beta)$ in Eq. (47), the following relationship holds

$$\sum_{\mu} \text{Tr}(q_{\mu}^{-1} dq_{\mu}) = \sum_{\mu} d \ln \det(q_{\mu}) \neq d \ln \det(\sum_{\mu} q_{\mu}), \quad (48)$$

thus suppose $\beta_{GBZ,1}$ coincides with $\beta_{GBZ,2}$, Eq. (47) cannot be reduced to the previous single GBZ cases as Eq. (44). To overcome this issue, we use the “wave function” method introduced in [52], which writes

$$\omega_{nojump} = \frac{1}{2}(\omega_+ - \omega_-), \quad \omega_{\pm} = -P_{\pm} + \sum_{\mu} Z_{\pm,\mu}, \quad (49)$$

where P_{\pm} is the order of the pole of $\det(h_{\pm})$, $Z_{\pm,\mu}$ is the number of the zeros that not only satisfy $\det(h_{\pm}(\beta)) = E_{\mu}(\beta) = 0$, but also being inside its corresponding sub-GBZ $_{\mu}$. The basic idea of this equation is a promotion of the multi-band winding number, and the proof of this formula requires *Cauchy's argument principle* [55]. When the zeros that do not belong to the band $E_{\mu}(\beta)$ pass through the corresponding GBZ $_{\mu}$, they will not contribute to the winding number. By using Eq. (46), $\det(h_+) = (\gamma^2 - 4(t_1 - it_2\beta)^2)/16$, $\det(h_-) = (\beta^2(\gamma^2 - 4t_1^2) - 8i\beta t_1 t_2 + 4t_2^2)/(16\beta^4)$, it is worth stressing that the zeros are all double degenerate, and we can also find $P_+ = 0, P_- = 4$. In Fig. 4(a),4(b) we denote all the zeros Z_{\pm} with blue (+) or green (-) dots. In Fig. 4(a), from the definition of Z_{\pm} , it is easy to find that the zeros ± 2 belong to GBZ $_1$ while ± 1 belong to GBZ $_2$. Since the zeroes $+1, +2$ are outside GBZ $_{2,1}$, they do not contribute to the total winding number, which means $Z_{+1,2} = 0$. Meanwhile, because of degeneracy, the zeros $-1, -2$ each correspond to $Z_{-2,1} = 2$, thus we have $\omega_{nojump} = 0$. Similarly, in Fig. 4(b), $Z_{+1,2} = 2, Z_{-1,-2} = 0$, and the total winding number $\omega_{nojump} = 4$.

Based on the following analysis, in Fig. 4(e), we plot the total wind number ω_{nojump} that changes with the intracell hopping strength t_1 . Comparing the result in Fig. 2(b),2(c) and Fig. 3(b),3(c), it is straightforward that open quantum description can predict the transition points as in NH systems. Although their model dimensions and used methods are totally different, the transition points appear at the same location. It proves the validity of our scheme in describing the phases of open systems, and may also help us to study the nature of the system when quantum jumps are involved.

When jumping terms are presented, from Sec. III, we have learned that the shape matrix A is time-reversal symmetric, thus its Bloch form satisfies

$$A(-k) = U_T A^*(k) U_T^{\dagger}, \quad (50)$$

where $U_T = I_2 \otimes \sigma_y \otimes \sigma_x$ is Hermitian and unitary. By choosing $\mathcal{P} = U_T$ and \mathcal{T} as the conjugation operator \mathcal{K} , we will have

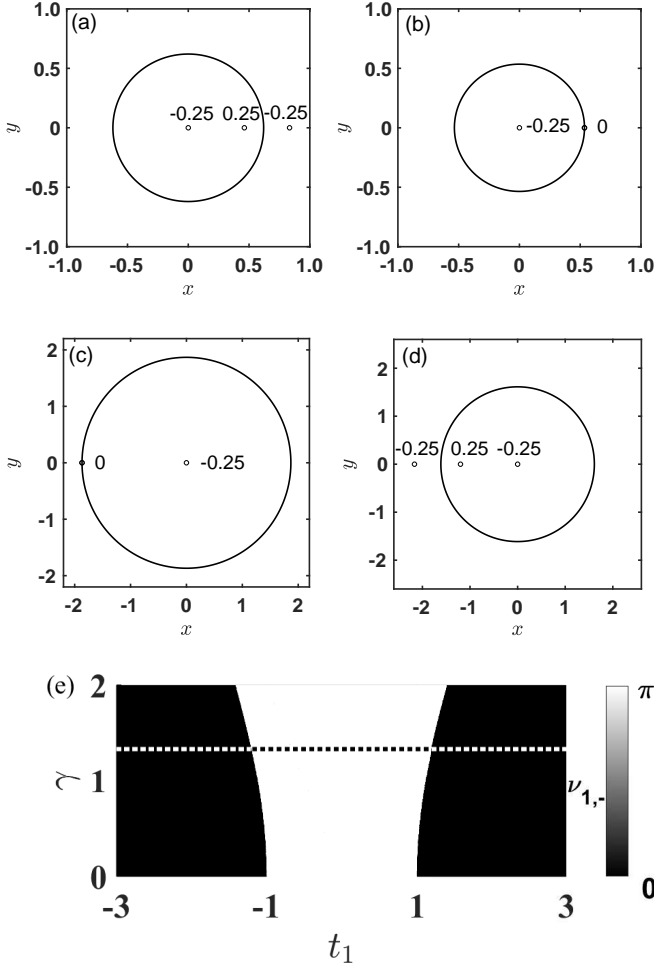


FIG. 5. (a-d) The GBZ of band $E_{1,-}$ when jumping terms are included. To show the differences and similarities, parameters are chosen as the same as in Fig. 3(a)-3(d). The number is the residue of the corresponding pole of zak phase $\nu_{1,-}$. The 0 residues in (b)(c) are the second order pole, while others are of the first order. (e) The phase diagram of zak phase $\nu_{1,-}$ respect with t_1 and γ , where κ takes 1. The black region corresponds to a 0 zak phase and the white region represents a π zak phase. The dashed line represents the previous set of parameters when $\gamma = 4/3$.

$\mathbf{A}(k)\mathcal{PT} = \mathcal{PT}\mathbf{A}(k)$. In other word, the shape matrix $\mathbf{A}(k)$ is \mathcal{PT} invariant under combined action of parity and time inversion, $[\mathbf{A}, \mathcal{PT}] = 0$. The corresponding topological phases in 1D system is usually defined by zak phase [56], which can be regarded the analogue of the Berry phase that the particle picks up when moving across the Brillouin zone. In closed systems, it is proved by Hatsugai *et al.* that the zak phase takes integer multiples of π in the presence of \mathcal{PT} symmetry [57]. With the introduction of the biorthogonal basis [58], the concept of the zak phase has been extended to NH systems [59], or Bloch Liouvillians [27]. In case of our model, we can define the zak phase of a given band as

$$\nu_\mu = i \oint_{\beta_{GBZ}} \langle l_\mu | \partial_\beta | r_\mu \rangle d\beta, \quad (51)$$

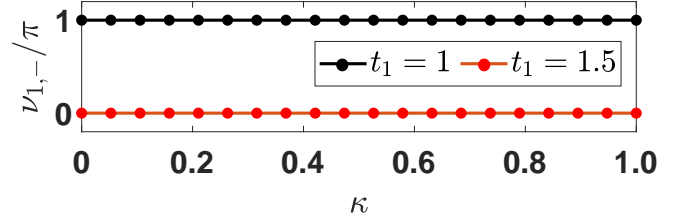


FIG. 6. The numerical result of the zak phase $\nu_{1,-}$ corresponding to $E_{1,-}$ band, which respects to different jump parameters κ . The black line and dots represent $t_1 = 1$ case, while the red represent $t_1 = 1.5$. The zak phase is unchanged under different values of κ . The other parameters are chosen as $t_2 = 1$, $\gamma = 4/3$.

where β_{GBZ} is the GBZ of the selected band, the $|l_\mu\rangle$ and $|r_\mu\rangle$ are the left and right eigenvectors of $\mathbf{A}(\beta)$, associated with the eigenvalue E_μ (Eq. (20)).

As an example, in Fig. 5(a)-5(d), we plot the GBZ of the band $E_{1,-}$ when jump is presented ($\kappa = 1$). The parameters are chosen as the same in the previous subsection. By using Eq. (51), we can obtain the analytical zak phase of $E_{1,-}$ band

$$\nu_{1,-} = i \oint_{\beta_{GBZ,E_{1,-}}} \frac{t_2(2\beta^2(t_1 - \gamma/2) + 4\beta t_2 + 2t_1 + \gamma)}{2\beta(\beta(\gamma - 2t_1) - 2t_2)(\gamma + 2(t_1 + \beta t_2))}, \quad (52)$$

where $\beta_{GBZ,E_{1,-}}$ is the closed loop restricted by Eq. (37a),(37b), by combing the two equations Eq. (20) and Eq. (B4), corresponding to the band $E_{1,-}$. In this way, the zak phases for all bands can be calculated.

In Fig. 5(e), we display the phase diagram describing the dependence of zak phase $\nu_{1,-}$ on t_1 and γ , where the black and white region contributes a 0 or π phase respectively. We can find that in the full area the zak phase is quantized, which is in contrast to previous studies, that only appears in \mathcal{PT} -unbroken regimes [27, 60, 61]. The transition points are $t_1 = \pm \sqrt{(\gamma/2)^2 + t_2^2}$, and the dashed line stands for $\gamma = 4/3$ in Fig. 5(a)-5(d).

Finally, in order to visualize the effect of quantum jump events, by numerically solving Eq. (51), we show $\nu_{1,-}$ as a function of κ . Intriguingly, the jump does not influence the conclusions above, which indicates that the model has κ independent zak phase. One may expect that the quantum jump will not affect the winding number of the entire system, however, it is a model-dependent issue. For the sake of simplicity, in the above analysis, we only considered loss in Fig. 1(a). It leads to the fact that when writing the Liouvillian operator \mathcal{L} in the matrix representation (Fock space), the jump induced Liouvillian $\kappa \mathcal{L}_{jump}$ will map states in the subspaces labeled by (N_a, N_b) to $(N_a - 1, N_b - 1)$, where N_a, N_b are the numbers of excited fermions; while the other parts $\mathcal{L}_{without jump} = \mathcal{L}_0 + \mathcal{L}_{eff}$, will not perform projections of states to other subspaces. Mathematically, the jump absence terms $\mathcal{L}_{without jump}$ can be written as block-diagonal forms, and the jumping terms $\kappa \mathcal{L}_{jump}$ could be encoded as block-upper-triangular forms. The latter will not affect the Liouvillian spectrum $\{\Lambda\}$, regardless of PBC or OBC [17, 23]. The consistency of the full Liouvillian spectra of $\mathcal{L}_{full} = \mathcal{L}_{without jump} + \kappa \mathcal{L}_{jump}$ (red circles)

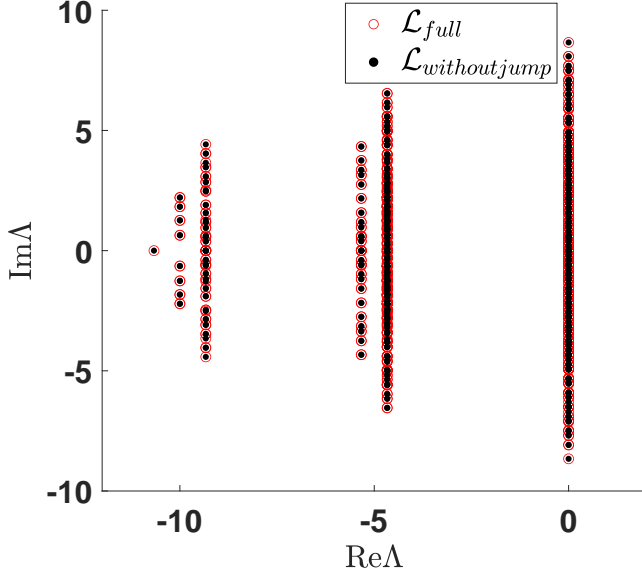


FIG. 7. Numerical result of the Liouvillian spectrum $\{\Lambda\}$ of our model, the calculation is based on the exact diagonalization method in Ref. [62]. The red circles represent the \mathcal{L}_{full} and the black dots are for $\mathcal{L}_{without_jump}$. We restrict the maximum excitation of subspaces with $\text{Max}N_a, N_b = 2$, and parameters are set to $t_1 = 1.5, t_2 = 1, \gamma = 4/3, \kappa = 1, N = 8$.

and $\mathcal{L}_{without_jump}$ (black dots) in Fig. 7 prove our conjecture.

In addition, the following conclusion also means their rapidities of the shape matrix are all the same (actually, for PBC, we have already shown that they are the same, as in Eq. (20)), because the Liouvillian spectrum is a linear combination of the rapidities [36]. According to the characteristic equation Eq. (40a),(40b), the same spectrum induces the same region of GBZ, which does not depend on the change of κ .

For a more visual demonstration of the unique effects of quantum jumps, we show a circumstance that the GBZ depends on jump strength κ , when the system not only loss (Eq. (3a)) but also gain particles (Eq. (3b)). Such constructions are general, such as achieving non-trivial nonequilibrium steady state (NESS) [34] or Liouvillian skin effect [35]. In these cases, the jumping terms cannot be written as upper triangular block forms as before, which may indicate that they are non-negligible.

We re-calculate the GBZ in the presence of gain, and in particular, $\kappa = 1$, the sub-GBZ is still a circle, whose radius r is

$$r = \left| \frac{\gamma_l/2 - \gamma_g/2 + t_1}{\gamma_l/2 - \gamma_g/2 - t_1} \right|^{\pm \frac{1}{2}}. \quad (53)$$

It can be seen that the difference between γ_l and γ_g determines the contour of GBZ, while in the effective theory their sum does (Eq. (4)). Moreover, when κ takes other values, the GBZ may no longer be a circle. In these cases, the jumping terms can not be safely neglected, which is different from the circumstance when there is only loss. In Fig. 8, we display the zak phase for the case when the system has both loss

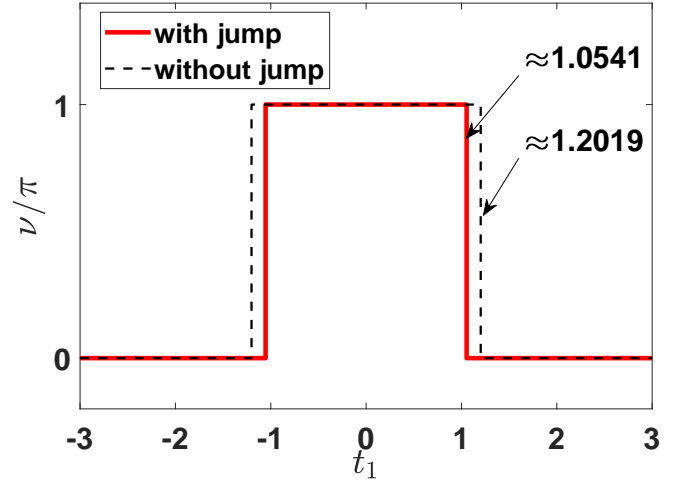


FIG. 8. The zak phase ν of a selected band when the system is suffering both loss and gain ($\kappa = 1$, red solid line), and the jumping absence case ($\kappa = 0$, black dashed line, as discussed in the main text). The transition points changed, which indicates that the jumping terms can not be safely neglected. Parameters are chosen as $t_2 = 1, \gamma_l = 1, \gamma_g = 1/3$.

and gain (red solid line), the jump absence result (the black dashed line) is also plotted for a comparison. The transition points $t_1 = \pm \sqrt{t_2^2 + ((\gamma_l - \gamma_g)/2)^2}$ are shifted, in contrast to the previous conclusion.

To summarize, the effect of quantum jumping events in the system needs to be carefully examined and may significantly affect the conclusions in effective NH systems, which demonstrates the necessity of our scheme.

Bulk-edge correspondence

In this subsection, we will show that the bulk-edge correspondence still holds in our scheme. The OBC spectra $\{\lambda\}$ of \mathbf{A}' is numerically calculated in Fig. 9(a)-9(b) ($\gamma_g = 0$), apparently we can observe eight degenerated edge states ($\text{Im}\lambda = 0$). According to Fig. 4(e), the invariants (0 or 4) and edge states (0 or 8) show one-to-one correspondence with each other. The bulk-boundary correspondence is fulfilled, since the system possesses two boundaries. The same conclusion holds for \mathbf{A} , with a total zak phase (0 or 8π), by using Eq. (51).

VI. CONCLUSION

In this work, we develop a new approach to study the topological properties by utilizing the third quantization technique, and study an SSH lattice with collective loss and gain as an example. When quantum jumping terms are neglected, by analyzing the property of the shape matrix, we find our scheme is consistent with the conventional approach in many aspects. In addition, the topological properties in the presence of quantum jumping terms are also studied. In this circumstance, due

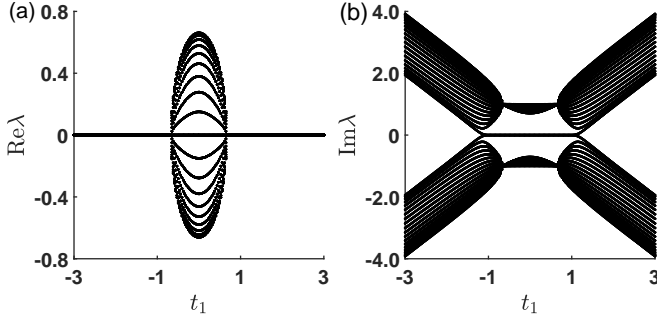


FIG. 9. (a-b) The real (a) and imaginary part (b) of numerical spectra $\{\lambda\}$ of the shape matrix \mathbf{A}' with an open chain, here we choose $N = 20$, $t_2 = 1$, and $\gamma = 4/3$, t_1 varies from -3 to 3 .

to the involvement of quantum jumps, the topological transition points may shift. Our work reveals the unique role of quantum jump terms between NH systems and master equations, which can not be neglected and explained by the effective Hamiltonian theory.

ACKNOWLEDGMENTS

We thanks Professor X.X.Yi for his helpful discussions. This work was supported by the National Natural Science Foundation of China (NSFC) under Grants No. 12175033, No. 12147206 and National Key R&D Program of China (No. 2021YFE0193500).

Appendix A: THE AZ SYMMETRY CLASSIFICATION

Class	A	AIII	AI	BDI	D	DIII	AII	CII	C	CI
T	0	0	+	+	0	-	-	-	0	+
C	0	0	0	+	+	+	0	-	-	-
S	0	1	0	1	0	1	0	1	0	1

TABLE I. AZ Classification of symmetries, T,C,S represent the symmetry of time reversal, particle hole and chiral. The 0 or 1 means the absence or presence of the symmetry, while the signs \pm indicate the $U_{T,C}U_{T,C}^* = \pm I$.

Appendix B: THE CALCULATION OF GENERALIZED BRILLOUIN ZONE

The calculation of the generalized Brillouin zone in the main text is basically based on the scheme proposed in Ref. [2, 13], where the usually used BZ in Hermitian case can be considered as its special circumstance. Here we give out a brief outline for the calculation of GBZ.

(i) Suppose a 1D tight-binding model with total dimension $2M$, the Hamiltonian is given by

$$H = \sum_{n,i,\mu,\nu} t_{i,\mu\nu} c_{n+i,\mu}^\dagger c_{n,\nu}, \quad (\text{B1})$$

where n represents the n th cell of the model, μ, ν is the index of the fermion in an individual cell, which may contain multiple degrees like momentum, spin, etc. t is the hopping strength and different i indicates the long-range interactions of lattices in different cells.

(ii) The eigen-function of Hamiltonian satisfies $H|\Psi\rangle = E|\Psi\rangle$, the eigenvector $|\Psi\rangle$ in the real space can be written as a linear combination

$$|\Psi\rangle = (\dots, \psi_{n,1}, \psi_{n,2} \dots \psi_{n+1,1} \dots)^T, \quad (\text{B2})$$

$$\psi_{n,\mu} = \sum_j \phi_{n,\mu}^{(j)} \phi_{n,\mu}^{(j)} = (\beta_j)^n \phi_{m,\mu}^{(j)}, \quad (\text{B3})$$

where Eq. (B3) is because of spatial periodicity.

(iii) After simplification, the characteristic equation of the Bloch form Hamiltonian $\mathcal{H}(\beta)$ can be presented as

$$f(\beta, E) = \det(\mathcal{H}(\beta) - E) = \frac{P(\beta, E)}{\beta^p} = 0, \quad (\text{B4})$$

where $\mathcal{H}(k)$ is performed by a substitution $e^{ik} \rightarrow \beta$. The norm of β is usually not necessarily unity, which is the reason why the ordinary Brillouin zone breaks down in NH cases. The p denotes the order of the pole of $P(\beta, E)$, and $f(\beta, E)$ can be trivially factorized as

$$f(\beta, E) = \prod_{\mu}^n (E - E_{\mu}(\beta)) = 0, \quad (\text{B5})$$

for multi bands, here n is the dimension of Bloch Hamiltonian \mathcal{H} .

(iv) Numerically calculate the eigenvalues E_i ($i=1,2,\dots,2M$) of H , and the β can be solved by function

$$f(\beta, E_i) = 0, \quad (\text{B6})$$

apparently, there are $2M$ solutions of β . To pick out the values of β , an important feature is the bulk-band property. For the solution labeled as $|\beta_1| \leq |\beta_2| \leq \dots \leq |\beta_{2M}|$, the continuum bands require a pair of β that satisfy

$$|\beta_M| = |\beta_{M+1}|, \quad (\text{B7})$$

which determine the trajectory of GBZ. In other word, there must exist a pair of conjugate points $\beta_M = \beta_0, \beta_{M+1} = \beta_0 e^{i\theta}$, where β_0 is a complex number. When H is Hermitian, it can be easily proved that GBZ is always a unit circle (Brillouin zone) [13].

Appendix C: THE MULTI GBZ CASES

With the help of *resultant*, we obtain the aGBZ of the shape matrix \mathbf{A}' in Sec. IV, the next urgent task is to verify the actual

area of GBZ. In Appendix B, we have known that the OBC spectrum $\{E\}$ is required in order to obtain the information of GBZ. However, we eliminate the degree E in Eq. (31), the values that can be taken from the energy spectrum $\{E\}$ is bounded, it may induce the GBZ usually a subset of aGBZ. To overcome this property, Ref. [52] puts up with the concept of a new kind of singularity point, self-conjugate points, that only occur in non-Hermitian systems, and the contours of aGBZ that possess the self-conjugate point must form GBZ. Recall that the Van Hove singularity k_s in Hermitian system [63], which satisfies

$$\partial_k E_\mu(k_s) = 0. \quad (\text{C1})$$

Since β is an extension of k , the generalized critical points

β_0 in NH system satisfy

$$\partial_k E_\mu(\beta_0) = 0. \quad (\text{C2})$$

In order to search the singularity points in all bands, we can use

$$f(E_0, \beta_0) = 0, \quad (\text{C3})$$

where E_0 satisfies

$$\begin{cases} f(E_0, \beta) = 0, \\ \frac{\partial f(E_0, \beta)}{\partial \beta} = 0, \end{cases} \quad (\text{C4})$$

it is proved that such self-conjugate points $\beta_M, \beta_{M+1} \in \{\beta_0\}$ not only have $|\beta_M| = |\beta_{M+1}|$, but also $\beta_M = \beta_{M+1}$ [52].

-
- [1] Carl M. Bender, “Making Sense of Non-Hermitian Hamiltonians,” *Reports on Progress in Physics* **70**, 947–1018 (2007).
 - [2] Shunyu Yao and Zhong Wang, “Edge States and Topological Invariants of Non-Hermitian Systems,” *Physical Review Letters* **121**, 086803 (2018).
 - [3] Wen-Tan Xue, Yu-Min Hu, Fei Song, and Zhong Wang, “Non-Hermitian Edge Burst,” *Physical Review Letters* **128**, 120401 (2022).
 - [4] Zhihao Xu and Shu Chen, “Topological Bose-Mott insulators in one-dimensional non-Hermitian superlattices,” *Physical Review B* **102**, 035153 (2020).
 - [5] Tsuneya Yoshida, Koji Kudo, and Yasuhiro Hatsugai, “Non-Hermitian fractional quantum Hall states,” *Scientific Reports* **9**, 16895 (2019).
 - [6] Tony E. Lee, “Anomalous edge state in a non-hermitian lattice,” *Phys. Rev. Lett.* **116**, 133903 (2016).
 - [7] Kai Li and Yong Xu, “Non-hermitian absorption spectroscopy,” *Phys. Rev. Lett.* **129**, 093001 (2022).
 - [8] Emil J. Bergholtz, Jan Carl Budich, and Flore K. Kunst, “Exceptional Topology of Non-Hermitian Systems,” *Reviews of Modern Physics* **93**, 015005 (2021).
 - [9] Xiao-Ran Wang, Cui-Xian Guo, and Su-Peng Kou, “Defective edge states and number-anomalous bulk-boundary correspondence in non-Hermitian topological systems,” *Physical Review B* **101**, 121116 (2020).
 - [10] Chuanhao Yin, Hui Jiang, Linhu Li, Rong Lü, and Shu Chen, “Geometrical meaning of winding number and its characterization of topological phases in one-dimensional chiral non-Hermitian systems,” *Physical Review A* **97**, 052115 (2018).
 - [11] Ye Xiong, “Why does bulk boundary correspondence fail in some non-hermitian topological models,” *Journal of Physics Communications* **2**, 035043 (2018).
 - [12] Yuto Ashida, Zongping Gong, and Masahito Ueda, “Non-Hermitian physics,” *Advances in Physics* **69**, 249–435.
 - [13] Kazuki Yokomizo and Shuichi Murakami, “Non-Bloch Band Theory of Non-Hermitian Systems,” *Physical Review Letters* **123**, 066404 (2019).
 - [14] Crispin Gardiner, Peter Zoller, and Peter Zoller, *Quantum noise: a handbook of Markovian and non-Markovian quantum stochastic methods with applications to quantum optics* (Springer Science & Business Media, 2004).
 - [15] Fabrizio Minganti, Adam Miranowicz, Ravindra W. Chhajlany, and Franco Nori, “Quantum exceptional points of non-Hermitian Hamiltonians and Liouvillians: The effects of quantum jumps,” *Physical Review A* **100**, 062131 (2019).
 - [16] Kazuki Yamamoto, Masaya Nakagawa, Kyosuke Adachi, Kazuaki Takasan, Masahito Ueda, and Norio Kawakami, “Theory of Non-Hermitian Fermionic Superfluidity with a Complex-Valued Interaction,” *Physical Review Letters* **123**, 123601 (2019).
 - [17] Xiangyu Niu, Jianning Li, S. L. Wu, and X. X. Yi, “Effect of quantum jumps on non-Hermitian system,” *arXiv:2202.12591* (2022).
 - [18] Klaus Mølmer, Yvan Castin, and Jean Dalibard, “Monte Carlo wave-function method in quantum optics,” *Journal of the Optical Society of America B* **10**, 524 (1993).
 - [19] Andrew J. Daley, “Quantum trajectories and open many-body quantum systems,” *Advances in Physics* **63**, 77–149 (2014).
 - [20] Juan Mauricio Torres, “Closed-form solution of Lindblad master equations without gain,” *Physical Review A* **89**, 052133 (2014).
 - [21] Fei Song, Shunyu Yao, and Zhong Wang, “Non-Hermitian skin effect and chiral damping in open quantum systems,” *Physical Review Letters* **123**, 170401 (2019).
 - [22] Stefano Longhi, “Unraveling the non-Hermitian skin effect in dissipative systems,” *Physical Review B* **102**, 201103 (2020).
 - [23] Tsuneya Yoshida, Koji Kudo, Hosho Katsura, and Yasuhiro Hatsugai, “Fate of fractional quantum Hall states in open quantum systems: Characterization of correlated topological states for the full Liouvillian,” *Physical Review Research* **2**, 033428 (2020).
 - [24] Wei Nie, Mauro Antezza, Yu-xi Liu, and Franco Nori, “Dissipative Topological Phase Transition with Strong System-Environment Coupling,” *Physical Review Letters* **127**, 250402 (2021).
 - [25] Clemens Gneiting, Akshay Koottandavida, A. V. Rozhkov, and Franco Nori, “Unraveling the topology of dissipative quantum systems,” *Physical Review Research* **4**, 023036 (2022).
 - [26] C-E Bardyn, M A Baranov, C V Kraus, E Rico, A İmamoğlu, P Zoller, and S Diehl, “Topology by dissipation,” *New Journal of Physics* **15**, 085001 (2013).
 - [27] Felix Dangel, Marcel Wagner, Holger Cartarius, Jörg Main, and Günter Wunner, “Topological invariants in dissipative extensions of the Su-Schrieffer-Heeger model,” *Physical Review*

- A **98**, 013628 (2018).
- [28] W.P. Su, JR Schrieffer, and Ao J Heeger, “Solitons in polyacetylene,” *Physical review letters* **42**, 1698 (1979).
 - [29] Fabrizio Minganti, Adam Miranowicz, Ravindra W. Chhajlany, Ievgen I. Arkhipov, and Franco Nori, “Hybrid-Liouvilian formalism connecting exceptional points of non-Hermitian Hamiltonians and Liouvillians via postselection of quantum trajectories,” *Physical Review A* **101**, 062112.
 - [30] Stephan Dürr, Juan José García-Ripoll, Niels Syassen, Dominik M Bauer, Matthias Lettner, J Ignacio Cirac, and Gerhard Rempe, “Lieb-liniger model of a dissipation-induced tonkgirardeau gas,” *Physical Review A* **79**, 023614 (2009).
 - [31] Yuto Ashida, Shunsuke Furukawa, and Masahito Ueda, “Quantum critical behavior influenced by measurement backaction in ultracold gases,” *Physical Review A* **94**, 053615 (2016).
 - [32] Zongping Gong, Sho Higashikawa, and Masahito Ueda, “Zeno Hall Effect,” *Physical Review Letters* **118**, 200401.
 - [33] Zongping Gong, Yuto Ashida, Kohei Kawabata, Kazuaki Takasan, Sho Higashikawa, and Masahito Ueda, “Topological Phases of Non-Hermitian Systems,” *Physical Review X* **8**, 031079 (2018).
 - [34] A. McDonald, R. Hanai, and A. A. Clerk, “Nonequilibrium stationary states of quantum non-Hermitian lattice models,” *Physical Review B* **105**, 064302 (2022).
 - [35] Fan Yang, Qing-Dong Jiang, and Emil J Bergholtz, “Liouvillian skin effect in an exactly solvable model,” *Physical Review Research* **4**, 023160 (2022).
 - [36] Tomaž Prosen, “Third quantization: A general method to solve master equations for quadratic open Fermi systems,” *New Journal of Physics* **10**, 043026 (2008).
 - [37] Alan A. Dzhioev and D. S. Kosov, “Nonequilibrium perturbation theory in Liouville-Fock space for inelastic electron transport,” *Journal of Physics: Condensed Matter* **24**, 225304 (2012).
 - [38] Manfred Schmutz, “Real-time green’s functions in many body problems,” *Zeitschrift für Physik B Condensed Matter* **30**, 97–106 (1978).
 - [39] Konstantin G. Zloschastiev and Alessandro Sergi, “Comparison and unification of non-Hermitian and Lindblad approaches with applications to open quantum optical systems,” *Journal of Modern Optics* **61**, 1298–1308 (2014).
 - [40] Alexander Altland and Martin R. Zirnbauer, “Nonstandard symmetry classes in mesoscopic normal-superconducting hybrid structures,” *Physical Review B* **55**, 1142–1161 (1997).
 - [41] Alexei Kitaev, “Periodic table for topological insulators and superconductors,” in *AIP conference proceedings*, Vol. 1134 (American Institute of Physics, 2009) pp. 22–30.
 - [42] Shinsei Ryu, Andreas P Schnyder, Akira Furusaki, and Andreas W W Ludwig, “Topological insulators and superconductors: Tenfold way and dimensional hierarchy,” *New Journal of Physics* **12**, 065010 (2010).
 - [43] Kohei Kawabata, Ken Shiozaki, Masahito Ueda, and Masatoshi Sato, “Symmetry and Topology in Non-Hermitian Physics,” *Physical Review X* **9**, 041015 (2019).
 - [44] Simon Lieu, Max McGinley, and Nigel R. Cooper, “Tenfold Way for Quadratic Lindbladians,” *Physical Review Letters* **124**, 040401 (2020).
 - [45] Yan He and Chih-Chun Chien, “Topological classifications of quadratic bosonic excitations in closed and open systems with examples,” *Journal of Physics: Condensed Matter* **34**, 175403 (2022).
 - [46] Shunyu Yao, Fei Song, and Zhong Wang, “Non-hermitian chern bands,” *Physical review letters* **121**, 136802 (2018).
 - [47] Flore K. Kunst, Elisabet Edvardsson, Jan Carl Budich, and Emil J. Bergholtz, “Biorthogonal Bulk-Boundary Correspondence in Non-Hermitian Systems,” *Physical Review Letters* **121**, 026808 (2018).
 - [48] Kohei Kawabata, Nobuyuki Okuma, and Masatoshi Sato, “Non-Bloch band theory of non-Hermitian Hamiltonians in the symplectic class,” *Physical Review B* **101**, 195147 (2020).
 - [49] Deguang Wu, Jiao Xie, Yao Zhou, and Jin An, “Connections between the open-boundary spectrum and the generalized Brillouin zone in non-Hermitian systems,” *Physical Review B* **105**, 045422 (2022).
 - [50] Kai Zhang, Zhesen Yang, and Chen Fang, “Correspondence between winding numbers and skin modes in non-hermitian systems,” *Physical Review Letters* **125**, 126402 (2020).
 - [51] Gang-Feng Guo, Xi-Xi Bao, and Lei Tan, “Non-Hermitian bulk-boundary correspondence and singular behaviors of generalized Brillouin zone,” *New Journal of Physics* **23**, 123007 (2021).
 - [52] Zhesen Yang, Kai Zhang, Chen Fang, and Jiangping Hu, “Non-Hermitian Bulk-Boundary Correspondence and Auxiliary Generalized Brillouin Zone Theory,” *Physical Review Letters* **125**, 226402 (2020).
 - [53] Ching-Kai Chiu, Jeffrey C. Y. Teo, Andreas P. Schnyder, and Shinsei Ryu, “Classification of topological quantum matter with symmetries,” *Reviews of Modern Physics* **88**, 035005 (2016).
 - [54] Ananya Ghatak and Tanmoy Das, “New topological invariants in non-Hermitian systems,” *Journal of Physics: Condensed Matter* **31**, 263001 (2019).
 - [55] Ruel Churchill and James Brown, *Ebook: Complex Variables and Applications* (McGraw Hill, 2014).
 - [56] J. Zak, “Berry’s phase for energy bands in solids,” *Physical Review Letters* **62**, 2747–2750 (1989).
 - [57] Yasuhiro Hatsugai, “Quantized Berry Phases as a Local Order Parameter of a Quantum Liquid,” *Journal of the Physical Society of Japan* **75**, 123601 (2006).
 - [58] Dorje C Brody, “Biorthogonal quantum mechanics,” *Journal of Physics A: Mathematical and Theoretical* **47**, 035305 (2014).
 - [59] Masatoshi Sato, Kazuki Hasebe, Kenta Esaki, and Mahito Kohmoto, “Time-Reversal Symmetry in Non-Hermitian Systems,” *Progress of Theoretical Physics* **127**, 937–974 (2012), arXiv:1106.1806 [cond-mat, physics:math-ph, physics:quant-ph].
 - [60] J.C. Garrison and E.M. Wright, “Complex geometrical phases for dissipative systems,” *Physics Letters A* **128**, 177–181 (1988).
 - [61] G Nenciu and G Rasche, “On the adiabatic theorem for nonself-adjoint Hamiltonians,” *Journal of Physics A: Mathematical and General* **25**, 5741–5751 (1992).
 - [62] J M Zhang and R X Dong, “Exact diagonalization: The Bose–Hubbard model as an example,” *European Journal of Physics* **31**, 591–602 (2010).
 - [63] Léon Van Hove, “The occurrence of singularities in the elastic frequency distribution of a crystal,” *Phys. Rev.* **89**, 1189–1193 (1953).
 - [64] Makio Kawasaki, Ken Mochizuki, and Hideaki Obuse, “Topological phases protected by shifted sublattice symmetry in dissipative quantum systems,” *Physical Review B* **106**, 035408 (2022).